Electron Acceleration and Transport in Microwave Flaring Loops

Victor F. Melnikov
Radiophysical Research Institute (NIRFI), Nizhny Novgorod 603950, Russia
meln@nirfi.sci-nnov.ru

Abstract

Nobeyama Radioheliograph has high spatial and temporal resolution at two frequencies where a nonthermal radio source is often optically thin. Such capabilities provide us with unique opportunity to get constraints on properties of mildly relativistic electrons accelerated and propagating in flaring magnetic loops. In this paper we review recent studies of Nobeyama observations concerning 1) spatial distribution of microwave brightness and spectral slope along flaring loops; 2) peculiarities of their temporal dynamics in different parts of a loop; 3) consequences of the obtained findings on spatial, spectral and pitch-angle distributions of high energy electrons.

Key words: the Sun: flares, microwave emission—particle acceleration and transport

1. Introduction

Spatial distribution of nonthermal emission along a single flare loop can bring us important information on the particle acceleration and transport. Studies of the microwave spatial distribution began in 80s using the WSRT and VLA facilities. The discovery of two kinds of microwave sources, single compact loop-top sources and double sources with their peaks located close to the conjugate magnetic footpoints (Marsh & Hurford 1980; Kundu et al. 1982; Kawabata et al. 1982; Nakajima 1983), stimulated the development of theoretical simulations of gyrosynchrotron brightness distribution along model magnetic loops (see Alissandrakis & Preka-Papadema (1984); Klein & Trottet (1984); Bastian, Benz & Gary (1998)). Later the similar studies were carried out using the Nobeyama Radioheliograph (NoRH) observations at single frequency 17 GHz (Hanaoka 1996; Nishio et al. 1997; Hanaoka 1999). They showed the existence of the double and triple radio sources associated with the footpoints of large and smaller flaring loops.

In recent years the new NoRH facilities have allowed to obtain images of solar flares at two high frequencies, 17 and 34 GHz, simultaneously with high angular ($5'' - 10''$) and temporal (0.1 s) resolution. These frequencies are remarkably higher than the usually observed spectral peak frequency, f_{peak} =5-10 GHz (Nita, Gary & Lee 2004), at which the optical thickness of gyrosynchrotron emission $\tau \approx 1$. This gives a chance to study the brightness distribution having the information on microwave spectrum slope, and, therefore, on the optical thickness in different parts of a flaring loop. Such high capabilities provide us with unique opportunity to get constraints on properties of mildly relativistic electrons accelerated and propagating in flaring magnetic loops.

Already the first reports on these two frequency observations (Melnikov et al 2001; Nindos et al 2001) gave quite unexpected results showing that at least in some events the bright looptop source is optically thin. This fact is in evident disagreement with the simulated brightness distribution of optically thin microwave emission along inhomogeneous magnetic loop. Several new studies were published during last years developing further understanding of the problem (Kundu et al. 2001; Melnikov, Shibasaki & Reznikova 2002a; Melnikov et al. 2002b; White et al. 2002; Lee et al. 2002; Lee et al. 2003; Karlicky & Kosugi 2004; Su & Huang 2004; Melnikov et al. 2005). Of special interest are new results concerning the spatial distribution and dynamics of the microwave spectral slope along flaring loops (Yokoyama et al. 2002; Melnikov et al. 2002b; Fleishman & Melnikov 2003; Zhou, Su & Huang 2005).

This paper is restricted to properties of single well resolved loop-like microwave sources. We review mainly our recent studies of Nobeyama observations concerning 1) spatial distribution of microwave brightness and spectral slope along flaring loops; 2) peculiarities of their temporal dynamics in different parts of a loop; 3) consequences of the obtained findings on spatial, spectral and pitch-angle distributions of high energy electrons. We show that detailed comparative analysis of the microwave brightness distribution along single magnetic loops using the new NoRH observations and model simulations gives us some new important constraints on the acceleration/injection mechanisms and kinetics of mildly relativistic electrons in solar flares.

2. Brightness distribution along extended flaring loops

The existence of the double and triple radio sources associated with the footpoints of flaring loops, as well as asymmetric sources, shown by Hanaoka (1996); Nishio et al. (1997); Hanaoka (1999), agrees well with the existing theoretical models of radio emission (Alissandrakis & Preka-Papadema 1984; Klein & Trottet 1984; Bastian, Benz & Gary 1998). The obvious reason of such the location is strong dependence of gyrosynchrotron intensity on

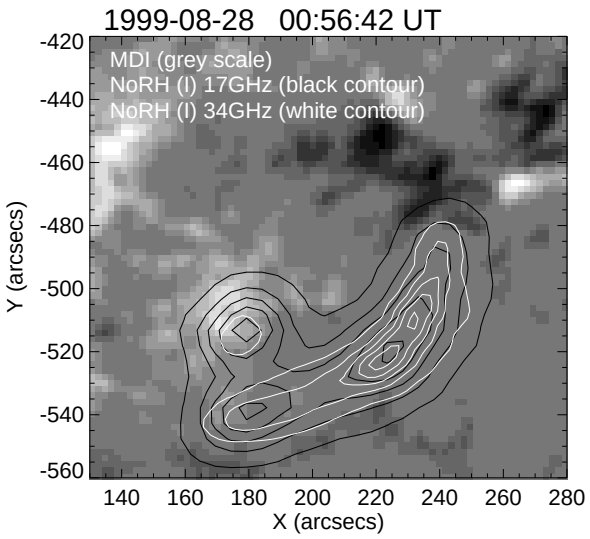

Fig. 1. SOHO/MDI photospheric magnetograms (gray scale) overlaid by contours of radio images at 0.1, 0.3, 0.5, 0.7 and 0.9 levels of the maximum brightness temperature (black for 17 GHz and white for 34 GHz). Magnetograms were obtained near the time of radio burst and were rotated to the moment of radio images.

magnetic field strength. On the other hand, the location of the brightness peak of optically thin microwave emission in the looptop is a challenge to our understanding of processes in flaring loops. In the next sections we will consider this problem in detail.

2.1. Spatial profiles of microwave brightness

For the detailed study of the spatial properties of microwave emission from a flare loop we selected only flares, which are characterized by the presence of well resolved extended single microwave sources and relatively simple time profiles both at 17 and 34 GHz. We have chosen the flares occured on 1999 August 28, 2000 January 12, March 13, 2001 October 23 and 2002 August 24. Their sizes (25-90 arc sec) exceed considerably the beam size of the Nobeyama Radioheliograph (NoRH) ($\Delta\varphi \sim 5''$ and $\sim 10''$ at 34 GHz and 17 GHz, respectively). The 1st, 3d and 4th flares occurred on the solar disk, the 2nd and 5th near the East and West limbs, respectively. The projections of the radio sources on the disk display a well developed loop-like structure at both frequencies. The limb source has an elliptic shape. Their peak brightness temperature varies from source to source from $7.0 \cdot 10^6$ K up to $1.2 \cdot 10^8$ K at 17 GHz and from $8.0 \cdot 10^5$ K up to $2.5 \cdot 10^7$ K at 34 GHz. The bursts show quite simple time profiles at 17 and 34 GHz with the duration of the main peaks in the range $\Delta T_{0.5} = 20 - 110$ s.

All the radio sources are optically thin at least at 34 GHz. Indeed, as analysis shows, the flux density spectral slope in the range 17-34 GHz is negative during the impulsive phase of the microwave bursts.

For the analysis of the microwave source structure we also used NoRH polarization maps as well as magnetographic data from SOHO/MDI. An example of overplotted NoRH and MDI maps is displayed on Fig.1. A loop like microwave source with the brightness maximum in its center is seen at 34 GHz map (white contours). Our analysis of MDI data has shown that the central part of the source is not associated with photospheric sunspots under the loop top. At the same time the MDI maps display the magnetic field enhancements of opposite polarities near two ends of the loop-like structures (supposed to be the indications of the loop footpoints).

The spatial profiles of the brightness along the loop-like radio sources at the peak time for each event are shown in the Fig.2. We can clearly see the brightness maxima to be located close to the central part of the sources. This is especially well pronounced for the highest frequency, 34 GHz, where the sources must be optically thin.

Note that the similar brightness distributions at the peak time of three limb flares observed with NoRH were obtained by Kundu et al. (2001). This proves that such kind of the brightness distribution for extended flaring loops is quite common and, therefore, should be studied in detail.

2.2. Time delays of the emission from different parts of a loop-like microwave source

In Fig.3a,b we show the flux time profiles from the regions corresponding to different parts of the loop source for the event on March 13, 2000: the loop-top (black contour in Fig.4b,c) and the north-east footpoint (white dashed-dotted contour at the same plots). Time profiles of the emission from the second footpoint are not shown here since their behavior is very similar. The size of the regions used for the flux calculations is 10" × 10".

It is well seen that the burst of emission from the loop top is delayed against the burst from the footpoint source by several seconds. This delay is more pronounced at 34 GHz than at 17 GHz. Furthermore, it is clearly seen that the time profiles of emission from the loop top are wider and their decay is slower than those from the region near the footpoint. We did not find any noticeable delay between time profiles at both frequencies from the conjugate footpoints.

The similar delays and differences in the characteristic decay time are observed for all the events from our sample (see, for instance, Fig.10 for the event of 28 Aug 1999). Note that the flux peaks from the footpoint sources are coincident in time with the flux peaks of hard X-ray emission (compare Fig.10 and Fig.11 where the vertical line indicates the moment of the hard X-ray emission peak, 00:56:42 UT).

2.3. Time delays of microwave emission at different frequencies

A comparison of the microwave time profiles of emission at the frequencies 17 and 34 GHz from the same parts of a loop-like radio source is shown on Fig.3c,d and Fig.10. One can clearly see that, for the main peak of the bursts, the emission at higher frequency, 34 GHz, is delayed against that at 17 GHz. This is well pronounced

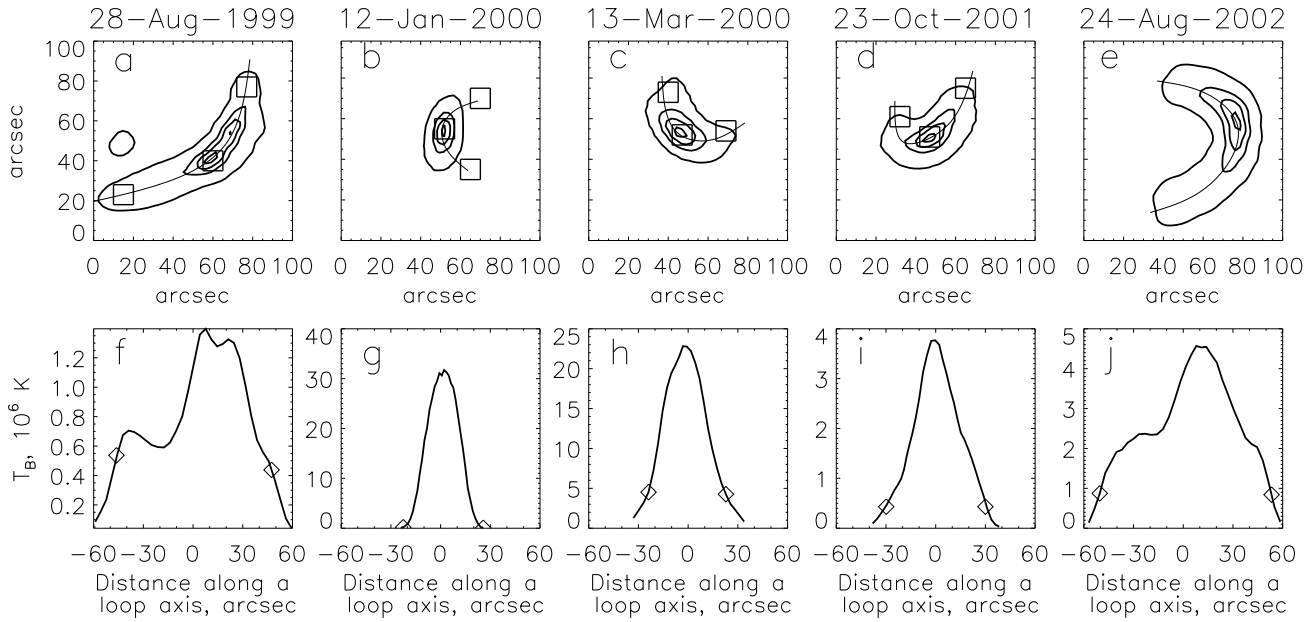

Fig. 2. *Top panel*: 34 GHz contour images of the sources at the moment of the bursts peaks (except e, this image is for the rise phase) for five events under study. Contours show 0.1, 0.5, 0.75 and 0.95 levels of the maximum brightness temperature. Thin curve shows the visible flaring loop axis. Three boxes of the size $10'' \times 10''$, two near footpoints and one near the loop-top show the areas which the flux time profiles were calculated from. *Bottom panel*: spatial distributions of radio brightness temperature at 34 GHz along a visible flaring loop axes shown on top panel for each event by thin curve. Zero position on the x-axes of bottom panel corresponds to the middle of the loop axis, calculated as a half of the axis length. Negative values corresponds to left footpoint on fig. a, c, d and lower footpoint on fig. b, e.

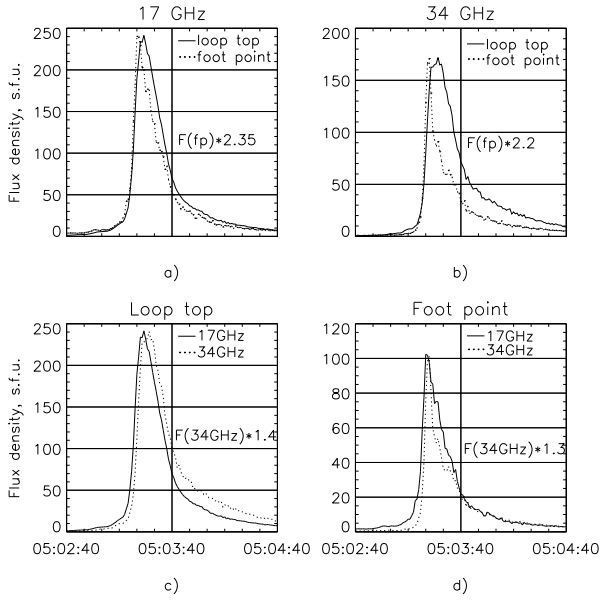

Fig. 3. NoRH time profiles of the flux densities from the 10"x10" boxes located at the loop top and the left footpoint (see Fig.4) of the flare 2000 March 13.

for the loop-top part of the sources. However there are no such delays for the footpoint parts. The footpoint emission at both frequencies reaches its maximum almost simultaneously with the peak of the corresponding hard X-ray burst (see Fig.10, 11).

2.4. Redistribution of microwave brightness along flaring loops

Further analysis of the microwave brightness distribution along the five well resolved flaring loops shows that it does not remain constant during a single peak of a burst (Melnikov et al. 2002b). In almost all the analyzed events there is the same tendency (see, for example, Fig.4). In the beginning of a burst there is always a time interval when brightness peaks (or one peak) are situated near the footpoints of a loop (both or only one). And close to the burst maximum or on the decay phase, an area near the looptop becomes most bright. A similar dynamics of brightness distribution was observed and studied in detail by White et al. (2002) in the event 1999 May 29.

To show this tendency more quantitatively, in Fig. 5 we compare the time profiles of fluxes and their ratios from the 10"x10" boxes, located near the left footpoint (a), right footpoint (c) and in the loop top (b) of the flaring loop in the event 2000 March 13. The location of the boxes are shown on Fig. 2(c). The *dotted* and *solid* lines correspond to the 17 and 34 GHz emission, respectively. The flux densities ratio F_{LT}/F_{FP} from the loop-top and

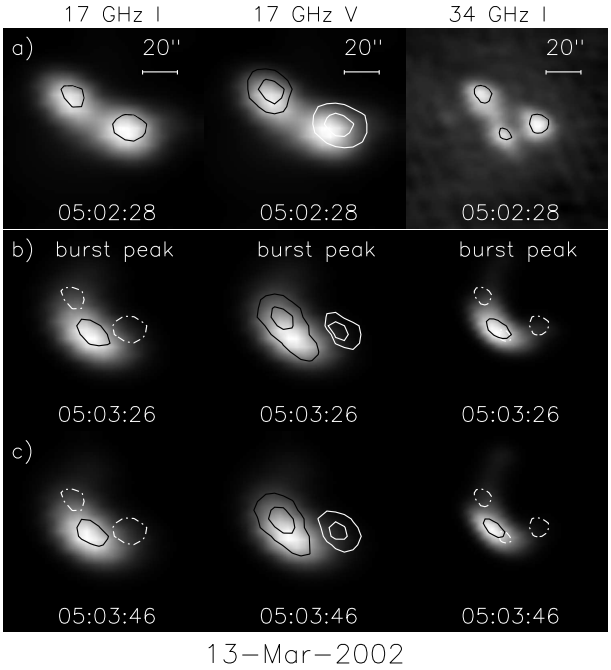

Fig. 4. NoRH images at the rise and peak phases of the flare 2000 March 13. Left and right panels: intensity at 17 and 34 GHz with the contours at the level 95% of the maximum at the current time (black solid line) and at the moment 05:02:28 UT (white dashed-dotted line). Middle panel: polarization V with the contours at the levels 40% and 80% of the maximum, black for positive V, and white for negative V.

the footpoint regions is calculated for the left footpoint (d) and for the right one (e). It is well seen that the ratios increase during the burst, especially fast on the early decay phase where maximum values of ratios reach 4-5.

Quite different evolution of the brightness distribution is realized during the limb event 2002 August 24. During the main peak of the burst, on its rising phase from 00:59:00, the southern footpoint of the loop becomes most bright at 34 GHz and remains the brightest part of the loop till the maximum at 01:00:30. At the peak time the brightness temperature reaches extremely high value at 34 GHz: $T_{Bmax} \approx 250$ MK. In Fig. 6a, b we can also see two other brightness peaks: one near the opposite (nothern) footpoint and one near the looptop. But they are much weaker. Only on the decay phase the looptop becomes relatively brighter then the footpoint sources which almost disappear to the moment of the valley before the second peak on the time profile (Fig. 6c, d). During the decay the brightness temperature in the southern footpoint source decreases by 5 times, and in the looptop only by 20%.

It is worth to note that during the main peak, when the total flux changes by 20-30 times, the visible size of the microwave flaring loop has almost not changed. It means that the emission flux changes entirely due to changes in number of mildly relativistic electrons in the loop but not in the area or volume of the source. More or less similar situation was observed for other flares from our set.

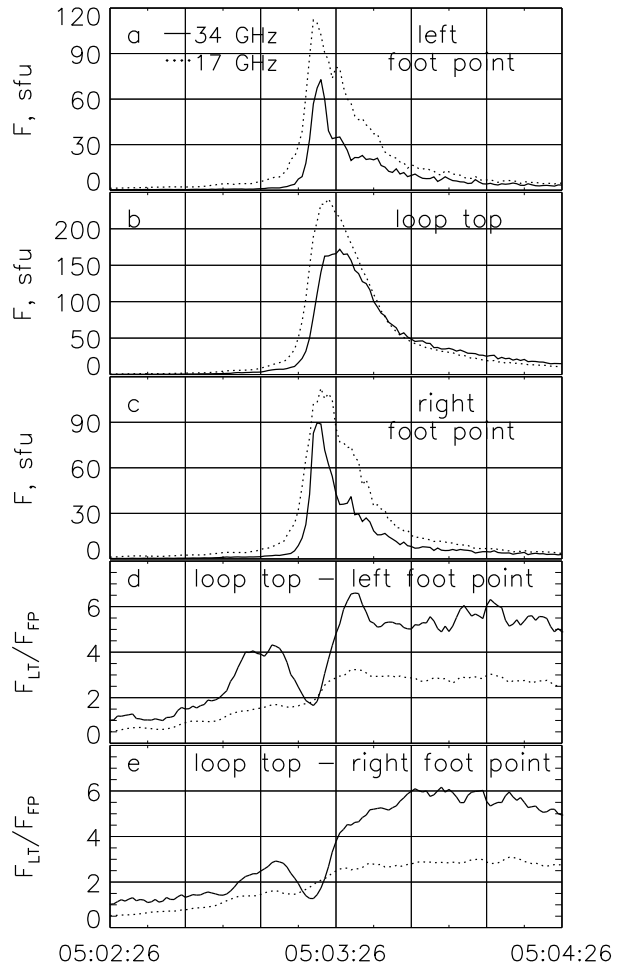

Fig. 5. NoRH time profiles of the flux densities from the 10"x10" boxes, located at the left footpoint (a), right footpoint (c) and in the loop top (b) of the flare 2000 March 13. The flux densities ratio F_{LT}/F_{FP} from the loop-top and the footpoint regions is calculated for the left footpoint (d) and for the right one (e).

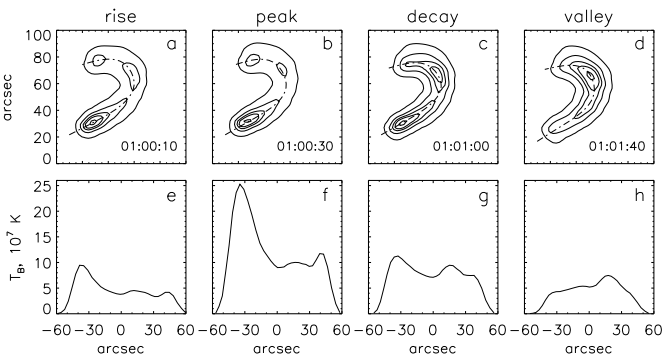

Fig. 6. Evolution of the brightness distribution during the limb event 2002 August 24.

2.5. *Comparison with the existing model predictions*

The most interesting feature of all the flares is that the peak of a microwave brightness distribution is located near the loop top at the burst maxima (except 2002 August 24).

This fact disagrees with the well known model simulations by Alissandrakis & Preka-Papadema (1984), and Klein & Trottet (1984) that predict the brightness peaks of optically thin emission to be near the footpoints of extended loops with a nonuniform magnetic field. The increase of the brightness temperature occurs because of the strong dependence of gyrosynchrotron intensity, I_f, on the magnetic field strength, B, that is expected to be larger near the feet of an extended loop. For example, if the electron power law spectral index $\delta = 4$, then according to Dulk (1985)

$$I_f \propto NB^{3.4}(\sin\theta)^{2.2}, \quad (1)$$

where N is the number of nonthermal electrons, θ is the viewing angle (angle between the magnetic vector and line of sight). It follows from the model by Alissandrakis & Preka-Papadema (1984) that even if an observer looks at a loop from above, the ratio of brightness temperatures in the loop top, I_{fLT}, and at the peak near footpoints, I_{fFP}, is equal to $I_{fLT}/I_{fFP} \simeq 0.5$ for the magnetic field difference $B_{LT}/B_{FP} = 1/2$. Note that the brightness peak near a footpoint is localized above the layers of strong chromospheric absorption, in the region where the view-angle $\theta \ll 90^\circ$, but is still not too small.

The striking fact is that the brightness peak at the looptop may be also observed for limb flares. For a limb loop which plane is almost perpendicular to the line of sight, $\theta = 80 - 90^\circ$, like for the events 2000 January 12 and 2002 August 24 from our set, the ratio is expected to be much lower for the same difference in magnetic strength: $I_{fLT}/I_{fFP} \sim 0.1 - 0.2$. As can be seen in Fig.2 (and also from the analysis of the limb events by Kundu et al. (2001); White et al. (2002)) the observable ratios at the highest frequency 34 GHz are just opposite: $I_{fLT}/I_{fFP} \sim 3 - 20$.

In the frame of the existing models such a strong increase of the brightness near the loop top is not possible to explain with usual assumptions on physical conditions in a flaring loop.

The possibility to have a hump in brightness near the loop top due to the effect of optically thick emission (Preka-Papadema & Alissandrakis 1992; Bastian, Benz & Gary 1998) is ruled out in our case since for all the events under study the frequency spectral index between 17 and 34 GHz is negative and, therefore, the microwave emission from the loops is optically thin at least at 34 GHz.

For loops near the solar disk center where the viewing angle θ is small near the footpoints the following two assumptions can make the loop top brighter than the footpoints. The first is constant magnetic field along the flaring loops (see Petrosian 1982 and Eq.(1)). The second is considerable transverse pitch-angle anisotropy of emitting electrons (Fleishman & Melnikov 2003; Fleishman 2005). The first assumption is problematic since the constancy of magnetic field strength along a loop suggests no trapping effect in contrast with our observations of well pronounced time delays (see sections 2.2- 2.3) in the analyzed events. The second assumption looks very probable. It is supported by observations of the spectral steepening toward footpoints that is also may be a consequence of the anisotropy (see section 3), as well as by the model simulations of electron distributions in flaring loops (see sections 2.6, 2.7).

For loops close to the limb with their plane almost perpendicular to the line of sight, the effects of both mentioned assumptions are too small to explain the observable ratios I_{fLT}/I_{fFP} and the shape of spatial profile along a loop (Kundu et al. 2001; White et al. 2002; Fleishman & Melnikov 2003).

2.6. Distribution of high energy electrons along a flaring loop.

We have to notice that the existing model simulations were made for the homogeneous distribution of energetic electrons along a loop. This assumption may strongly deviate from the reality. Indeed, the existence of delays (section 2.3) between the higher and lower frequency and hard X-ray intensity time profiles is an evident indication of electron trapping in microwave sources (Melnikov 1994; Melnikov & Magun 1998). The delays (section 2.2) between microwave emissions from the looptop and footpoints as well as longer decay of the emission from the looptop are a strong evidence of the trapping and accumulation of high energy electrons in the upper part of flaring loops.

A strong relative enhancement of energetic electron density near the looptop can eliminate the contradiction between the observations and the model predictions (Melnikov, Shibasaki & Reznikova 2002a). Under this assumption we can easily derive the magnitude of the electron number density enhancement from Eq.(1) and the observed ratios I_{fLT}/I_{fFP} mentioned in Section 2.5. The corresponding difference in the number densities in the loop top and footpoints falls in the range $N_{LT}/N_{FP} \sim 10 - 100$.

To illustrate this idea, Fig.7 displays three types of normalized spatial distributions along a loop. On the left hand the number density (dashed line) and column number density (solid line) electron distributions, and magnetic field distribution (dotted line) are shown. These types of electron spatial distributions are obtained in the collisionless case when the first adiabatic invariant constancy along a magnetic field line with nonuniform strength $B(s)$ is fulfilled: $[1-\mu^2(s)]/B(s) = const$, and the corresponding electron pitch-angle distributions in the loop center are taken to be (a) beam-like $\phi(\mu) = exp[-(1-\mu^2)/\mu_\parallel^2]$, with the beam width along magnetic field $\mu_\parallel = 0.3$, (b) isotropic (with taking into account the loss cone), and (c) pancake-like $\phi(\mu) = exp[-\mu^2/\mu_\perp^2]$, with the beam width transverse to magnetic field $\mu_\perp = 0.4$, where $\mu = cos\alpha_0$, α_0 - pitch-angle in the loop center.

The corresponding gyrosynchrotron intensity distributions along the model loop in optically thin regime (at 34 GHz) are shown on the right-hand panels of Fig. 7. The emission is calculated using the exact formalism (Ramaty 1969; Fleishman & Melnikov 2003). It is sup-

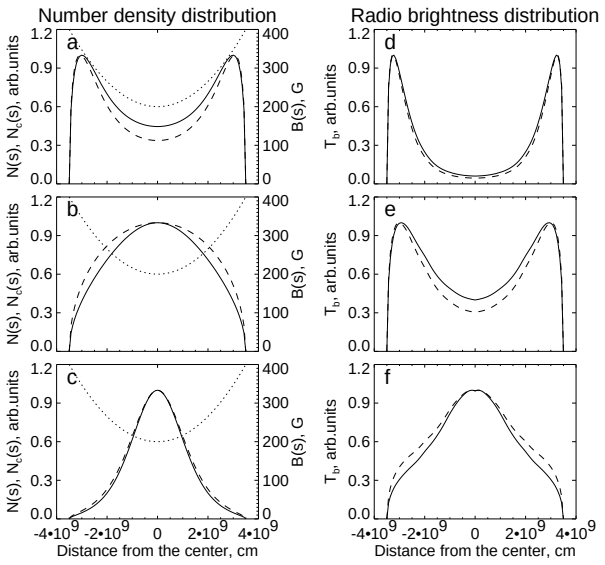

Fig. 7. Normalized spatial distributions along a loop (Melnikov et al. 2002a). Left column: number density (dashed line) and column number density (solid line) for the beam-like (a), loss-cone (b), and pancake (c) electron pitch-angle distributions; magnetic field distribution is shown by dotted line. Right column: corresponding gyrosynchrotron intensity in optically thin regime (at 34 GHz).

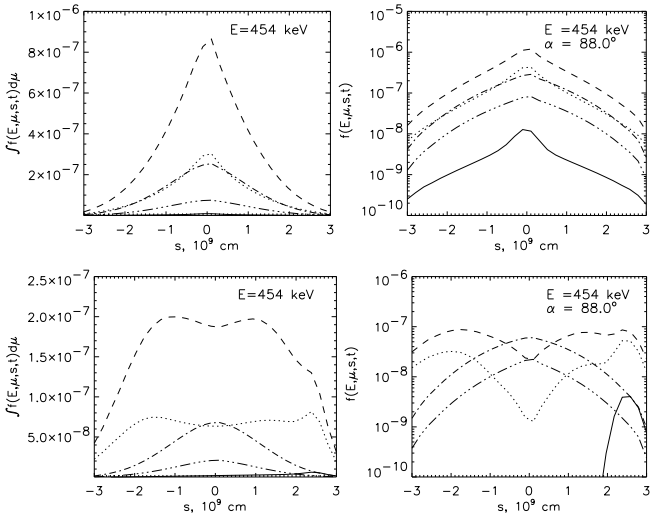

Fig. 8. Results of the model simulations using the Fokker-Planck equation (Gorbikov & Melnikov 2005). The distribution functions for the rising phase of injection are shown by solid ($t = 0.2$ s), dotted ($t = 1.7$ s) and dashed ($t = 3.25$ s) lines, and for the decay phase by dot-dashed ($t = 7.1$ s) and dot-dot-dot-dashed ($t = 10$ s) lines. Top panel represents the time evolution for Model 1 (the maximum of injection function is located in the center of the trap, $s = 0$), and bottom panel for Model 2 (the maximum of injection function is located near the foot, $s = 2.4 \times 10^9$ cm). On the left: the electron distribution function is integrated over all μ and displayed in linear scale. On the right: the distribution function is shown only for electrons with pitch-angle $\alpha = 88^o$.

posed that electrons have a power law energy dependence: $g(E) = g_0 E^{-\delta}$; the model loop is located close to the limb and the viewing angle $\theta = 80^o$. Two strong peaks of radio emission are observed for the beam-like and even for the loss-cone distribution, while the well defined peak of the number density exists in the loop center (see Fig.7a-d,b-e). Only in the case of the pancake distribution we can get a pronounced radio brightness peak at the center of a limb loop (Fig.7c-f). A degree of brightness concentration to the loop center (the ratio I_{fLT}/I_{fFP}) can vary in wide range depending on the parameter $\mu_\perp$ of the Gaussian distribution function.

2.7. Dynamics of electron spatial distribution

To understand the origin of peculiarities of microwave brightness distribution and its dynamics along different flaring loops we do modeling of the time evolution of electron spatial distribution along a magnetic loop by solving the non-stationary Fokker-Planck equation under different assumptions on the physical conditions in the loop and for different positions of the injection site (loop top, loop foot).

We consider the non-stationary Fokker-Planck equation in the form (Hamilton et al. 1990), which takes into account Coulomb collisions and magnetic mirroring:

$$\frac{\partial f}{\partial t} = -c\beta\mu\frac{\partial f}{\partial s} + c\beta\frac{dlnB}{ds}\frac{\partial}{\partial \mu}\left[\frac{1-\mu^2}{2}f\right]$$

$$+\frac{c}{\lambda_0}\frac{\partial}{\partial E}\left(\frac{f}{\beta}\right) + \frac{c}{\lambda_0\beta^3\gamma^2}\frac{\partial}{\partial\mu}\left[\left(1-\mu^2\right)\frac{\partial f}{\partial\mu}\right] + S, \qquad (2)$$

where $f = f(E, \mu, s, t)$ is electron distribution function of kinetic energy $E = \gamma - 1$ (in units of mc^2), pitch-angle cosine $\mu = cos\ \alpha$, distance from the flaring loop center s, and time t, $S = S(E, \mu, s, t)$ is injection rate, $\beta = v/c$, v and c are electron velocity and speed of light, $\gamma = 1/\sqrt{1-\beta^2}$ is Lorentz factor, $B = B(s)$ is magnetic field distribution along the loop, $\lambda_0 = 10^{24}/n(s)ln\Lambda$, $n(s)$ is plasma density distribution, $ln\Lambda$ is Coulomb logarithm. We conducted our numerical calculations for two cases using the method developed by Gorbikov & Melnikov (2005). In the first case (Model 1) the source of high energy electrons is located in the magnetic trap center $s = 0$, and in the second one (Model 2) near a trap foot $s = 2.4 \times 10^9$ cm. In both models the trap (loop) is symmetrical and its half-length is 3×10^9 cm and magnetic mirror ratio $B_{max}/B_{min} = 5$. Plasma density is homogeneous along the loop with $n(s) = 2.5 \times 10^{10}$ cm^{-3}. The injection function $S(E, \mu, s, t)$ is supposed to be a product of functions dependent only on one variable (energy E, cosine of pitch-angle μ, position s, and time t):

$$S(E, \mu, s, t) = S_1(E)S_2(\mu)S_3(s)S_4(t), \qquad (3)$$

where the energy dependence is a power law $S_1(E) = (E/E_{min})^{-\delta}$, $E_{min} = 30$ keV, with spectral index $\delta = 5$; pitch-angle distribution is isotropic $S_2(\mu) = 1$; time dependence is Gaussian $S_4(t) = exp[-(t - t_m)^2/t_0^2]$, $t_m = 2.5$ s, $t_0 = 1.4$ s; spatial distribution is also Gaussian. For Model 1: $S_3(s) = exp(-s^2/s_0^2)$, and for Model 2: $S_3(s) = exp[-(s - s_1)^2/s_0^2]$, where $s_0 = 3 \times 10^8$ cm, $s_1 = 2.4 \times 10^9$ cm.

The results of the model simulations are presented in Fig. 8 where one can see the time evolution of electron number density along the loop for electrons with energy $E = 454$ kev.

It follows from Fig. 8 that for the case of Model 1 the shape of the spatial distribution does not change much with time. During all the injection phases the distribution remains similar, with the peak located at the looptop. The simulation also reveals strong perpendicular anisotropy of the electron pitch-angle distribution in the loop. The degree of electron concentration near the looptop is strong enough to produce a peak of the microwave brightness distribution (compare with Fig. 7).

In the case of Model 2, the shape of the spatial distribution changes with time dramatically forming a sequence of distributions from double-peak in the beginning to single peak on the decay phase. The comparison with Fig. 7 shows that such distributions should produce two well pronounced radio brightness peaks near the footpoints in the beginning and maximum phases of a burst, and the brightness peak at the loop top in the decay phase of the burst.

2.8. Constraints on the particle acceleration/injection and kinetics

The findings considered above put some constraints on the particle acceleration/injection and kinetics of high energy electrons in flaring magnetic loops.

It follows from our analysis that the looptop peak of the electron distribution on the maximum phase of a burst may be produced if the injection region is located near the loop top. The injected pitch-angle distribution should be isotropic or anisotropic of the pancake type. Such kind of injection is considered in some acceleration/injection models (Somov and Kosugi (1997); Fletcher (1999); Petrosian et al. (2002)). Recently Jakimiec (2002), Somov & Bogachev (2003) and Karlicky & Kosugi (2004) developed models which consider a magnetic trap collapsing after reconnection and providing conditions for the betatron acceleration of electrons transverse to magnetic field lines. On the other hand, there are models suggesting the DC-electric field acceleration along the axes of a twisted loop or the stochastic MHD-turbulent cascade acceleration, in which the acceleration occurs along the magnetic field lines (see for a review Miller et al. (1997), Aschwanden (2002)). Our simulations show that this type of injection can not produce microwave brightness peak in the looptop during the main phase of injection. However, we can not exclude the chance of the looptop source formation due to pitch-angle scattering and accumulation of trapped electrons in the top part of a loop on the decay phase.

The results of sections 2.6 and 2.7 show that microwave brightness peaks near the footpoints of a loop is easy to get if the injection region is located near one of the footpoints. This conclusion is quite general, simulations reveal that it works for any pitch-angle distribution of injected electrons. It means that the acceleration mechanism itself is not very important, the main thing here is the position of the acceleration/injection region. We can conclude that in cases when microwave flaring loops show brightness maxima near footpoints (like for the event 24 August 2002 or the events observed by Hanaoka (1996); Nishio et al. (1997); Hanaoka (1999)), the acceleration may take place in the loop leg close to a footpoint. We have to note, however, that this explanation is not unique. The footpoint brightenings could be observed even if the acceleration takes place in the looptop. But in this case the injection should occur preferably along the loop axes ("beam-like" injection). To distinguish between the two possibilities we have to involve some other observational properties of the microwave flaring loop. For this some further detailed investigations are needed. A more rigid set of constraints can be obtained from a study of spatial/spectral dynamics of microwave/HXR-emissions.

3. Spectral properties of the microwave emission in flaring loops

Spectral features of mildly relativistic electrons accelerated in solar flaring loops can be studied using observations of their optically thin gyrosynchrotron microwave emission which spectrum can usually be described by the power law:

$$F_\nu \propto \nu^\alpha, \tag{4}$$

where F_ν and ν are the flux density and frequency, respectively.

One of the important findings related to this topic is the dynamic flattening of the frequency spectrum during the rise and decay phases of impulsive bursts in the cm-mm wavelengths (Melnikov & Magun 1998). In the majority of events such the spectral flattening on the decay phase of bursts is accompanied by the simultaneous spectral softening of the corresponding hard X-ray emission (Melnikov & Silva 2000). This striking difference in the spectral behavior was interpreted as the natural consequence of the non-stationary "trap+precipitation" model, which takes into account the energy spectrum hardening of trapped electrons due to Coulomb collisions as well as the difference between the spectral evolutions of injected/directly precipitated and trapped electrons. On the other hand, Lee & Gary (2000) have shown that the evolution of the pitch-angle distribution of non-thermal electrons in a flaring loop can play an important role in the interpretation of the microwave spectral flattening.

Till recently studies of the spectral evolution of optically thin microwave emission of solar flares were carried out for the full Sun observations without any spatial resolution. One has got only the spectral relationships averaged over a whole source. Consequently, the physical models of a radio source were quite simplified. They considered the electron energy spectral evolution in a flare loop as a whole not taking into account possible inhomogeneity of both magnetic field and plasma density along the loop. Evidently, a study of microwave spectral evolution in different parts of a flare loop on the base of observations with a good spatial resolution may provide us by new, additional information. This information may help us to de-

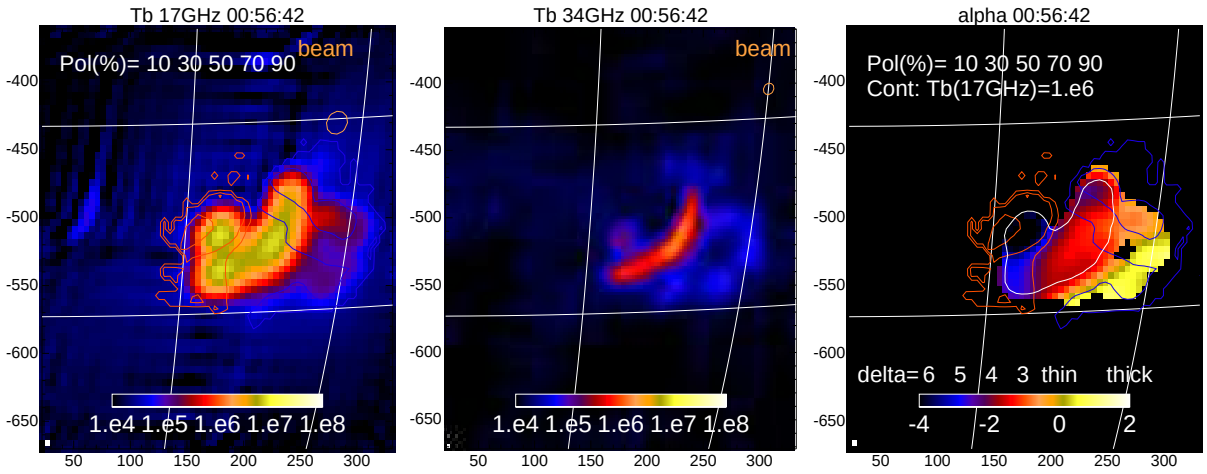

Fig. 9. Intensity and spectral slope distributions along the extended flaring loop in the event 28 August 1999 (Yokoyama et al. 2002). Left and middle panels: Microwave intensity (brightness temperature) map at 17 and 34 GHz obtained by NoRH in unit of Kelvin (color bar for the levels). Red and blue contours on the left panel indicate the polarization degree at levels of 10, 30, 50, 70, and 90 %. Beam size at half level of the peak intensity is shown as a brown circle at the right upper corner. Right panel: Map of microwave spectral slope α. The levels for each color are shown in the color bar, which is indexed below the bar with the values of α and is indexed above the bar with the power-law index of the electron distribution function δ derived by the Dulk's (1985) model. White contour indicates the level of the intensity of $T_{\rm b}$ =1 MK at 17 GHz. Blue and red contours are the same as those in the left panel.

velop a more appropriate physical model of a radio source and get better understanding of particle acceleration and transport in flare loops.

3.1. Spectral slope distribution along flaring loops

Nobeyama Radioheliograph provides us with observations at two high frequencies 17 and 34 GHz. So it gives unique possibility to study spectral slope's dynamics and its spatial distribution along flaring loops.

The parameter α described as

$$\alpha = \frac{ln(F_{34}/F_{17})}{ln(34/17)} \qquad (5)$$

characterizes the spectral slope between 17 and 34 GHz. For some extent this parameter can serve as an approximation to the frequency spectral index. This approximation is quite reasonable when the spectral peak of the emission is located at frequencies $f < 17$ GHz, which is the case for the events we discuss here. Note that due to the difference of the beam sizes at 17 and 34 GHz, the corresponding intensities F_{34} and F_{17} must be calculated after the adjustment of images at 17 and 34 GHz to the same antenna beam size. This is achieved by the convolution of the 17 GHz image with the 34 GHz beam and vice versa.

The very first study of the microwave spectral distribution along the extended flaring loop in the event 28 August 1999 (Yokoyama et al. 2002) has revealed very interesting regularity. The value of the radio spectral index is considerably higher (by approximately 1) in the footpoints than in the looptop. It is valid all the time during the main emission peak. This can be clearly seen in Fig.9 where distributions of intensity (left and middle panels) and spectral slope α (right panel) along the loop are shown. The color map of α and the color bar clearly indicate the increase of α near the footpoints of the loop. This regularity has been confirmed further in detailed studies of other extended flaring loops characterized by negative spectral slope between 17 and 34 GHz (Melnikov et al. 2002b; Zhou, Su & Huang 2005). New works by Takasaki et al (2005) and Kiyohara et al (2005) were also presented at Nobeyama Symposium 2004.

3.2. Microwave spectral evolution

A study of the microwave spectral evolution in different parts of five well-resolved loop-like radio sources (flares on 28 Aug 1999, 12 January 2000, 11 and 13 Mar 2000, 23 Oct 2001) were undertaken in the work by Melnikov et al. (2002b). For the analysis of these flares, hard X-ray data detected with the Yohkoh/HXT and the BATSE/CGRO hard X-ray spectrometers as well as magnetographic data from SOHO/MDI were also used. The frequency spectrum slope in the range 17-34 GHz during the impulsive phase of the bursts was negative throughout the sources extension. The common features found for all the events are as follows. The temporal evolution of α for different parts of a loop-like source, where it is optically thin (negative α), shows the very common behavior: a gradual increase of its value in the rise and decay phases of the bursts (for illustration see Fig. 10). This "soft-hard-harder" behavior of the microwave emission is associated with the "soft-hard-soft" behavior of the corresponding hard X-ray emission (Fig. 11). Such opposite evolution of the spectral slopes of the microwave and hard X-ray emissions on the decay phase is similar to the spectral evolutions of these emissions integrated over a whole source (Melnikov & Silva 2000).

Along with this it was found that the temporal increase of α (flattening of the microwave spectrum) during the

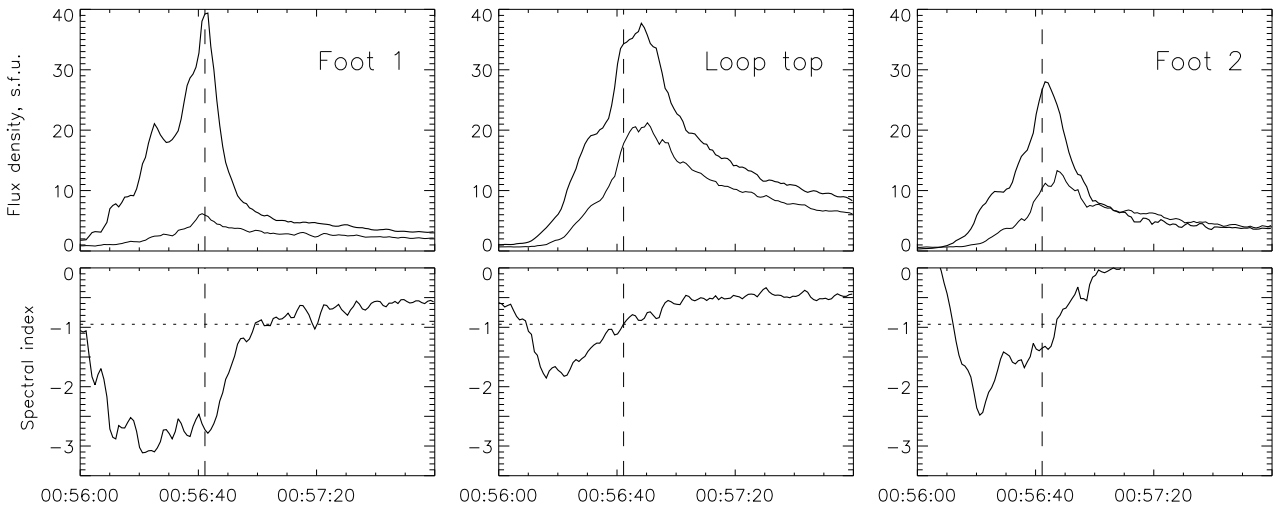

Fig. 10. Top panel: NoRH time profiles of the flux densities from the $20'' \times 20''$ boxes located at the loop top (middle panel) and the footpoints (left and right panels) of the flare 1999 August 28. Bottom panel: the corresponding time profiles of the spectral index calculated with equation (5). Vertical line indicates the moment of the hard X-ray emission peak, 00:56:42 UT.

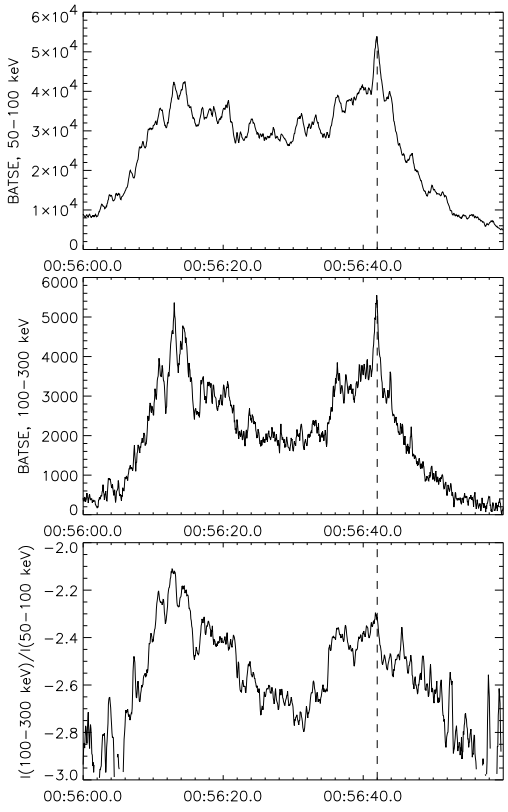

Fig. 11. Temporal profiles of hard X-ray emission during the event of 1999 August 28. Top and middle panels: Total fluxes at energy intervals $E_1 = 50-100$ keV and $E_2 = 100-300$ keV. Bottom panel: Flux ratio $I(E_2)/I(E_1)$ time profile corresponding the spectral index γ_x time profile of the hard X-ray spectrum $I(E) \propto E^{-\gamma_x}$. Vertical line indicates the moment of the emission peak at 00:56:42 UT.

decay phase goes remarkably faster in the regions close to the footpoints than near the loop top. In the event 28 August 1999 (see Fig.10), the index α changes from -2.7 to -1.0 and from -1.3 to -0.2 for the left and right loop footpoints, respectively, whereas from -1.0 to -0.6 for the looptop during the interval of 20 s after HXR-peak.

3.3. Possible physical reasons of the spectral properties

We see four possible reasons for the observed difference in spectral slopes between the looptop and footpoints regions.

The first one is associated with a perpendicular anisotropy of the electron pitch-angle distribution. Due to stronger directivity of gyrosynchrotron emission at higher frequencies the anisotropic distribution provides systematically steeper frequency spectra at quasi-parallel directions than at quasi-transverse directions (Fleishman & Melnikov 2003). This reason may well work for disk flares since for them the foot-point source is observed at a quasi-parallel direction, while the loop-top source in quasi-transverse. In the left bottom panel of Fig. 12 one can see that in the optically thin regime, at $f > f_{peak}$, the spectral index considerably (by 0.5 to 1) increases with the degree of anisotropy (change of the loss-cone angle θ_c from 0 to $\pi/2$), while it is almost constant in the case of quasi-transverse propagation (the right bottom panel).

Note that the effect of the anisotropy is expected to be less pronounced for limb flaring loops (though this depends on a specific difference between the electron pitch-angle distributions in the looptop and footpoints). Meanwhile, sometimes one observes the same spectral slope distribution also for limb flares (Melnikov et al. 2005). The following effects are free of this limitation.

The second reason is the influence of magnetic field strength on the frequency spectral slope around a fixed frequency. An increase of spectral index at lower harmonics is a general feature of gyrosynchrotron emission from a power law electron energy distribution in the case

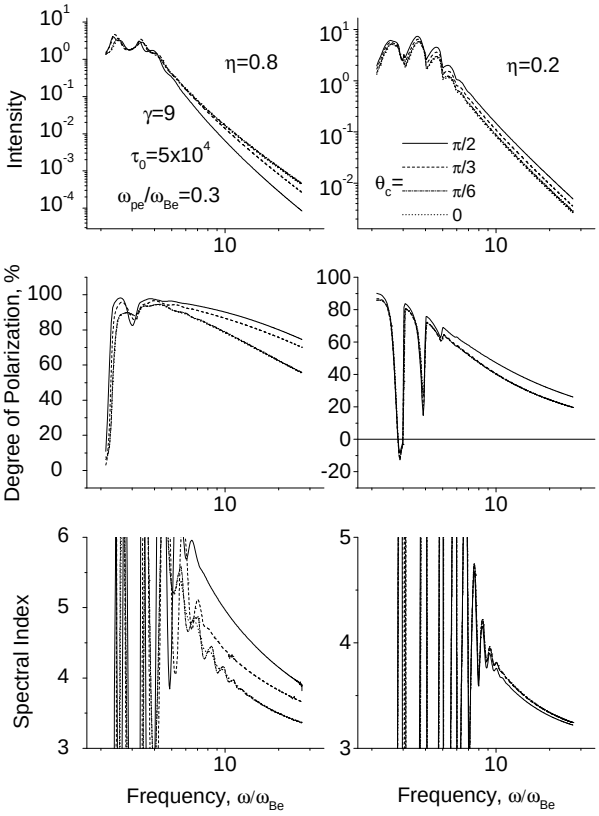

Fig. 12. The gyrosynchrotron radiation intensity, degree of polarization and spectral index vs frequency for various loss–cone angles θ_c in sin-N pitch-angle distribution (Fleishman & Melnikov 2003). The decrease of intensity and increase of spectral index with θ_c are clearly seen for the quasi-parallel propagation ($\eta = 0.8$). The increase of spectral index at lower harmonics is also well pronounced.

of low density plasma $\omega_{pe} < \omega_{Be}$. The increase from the relativistic limit ($\alpha_{rel} = (\delta - 1)/2$) that is realized at harmonic number $\omega/\omega_{Be} \geq 100$ may reach 0.5-1 as can be seen on bottom left and right panels in Fig.12. In a footpoint the magnetic field strength is expected to be higher than in the loop top. Therefore, the corresponding emission at a given frequency is generated at a lower harmonics and with a steeper spectrum.

Another effect that may greatly influence the spectral slope at frequencies $f > f_{peak}$ is Razin suppression (Razin 1960). Due to this effect the spectral index α may be considerably (by 0.5-2) smaller than even α_{rel} if the parameter ω_{pe}/ω_{Be} in the source is sufficiently high (Fleishman & Melnikov 2003). Since this parameter has to be larger in the looptop than near footpoints due to weaker magnetic field strength, we expect a spectral flattening in the looptop. A detailed diagnostics of flare plasma shows that this effect may be the main one at least for some flares (Melnikov et al. 2005). In Fig.13 one can clearly see that due to enhanced Razin suppression in the top part of the flaring loop the spectral peak shifts to higher frequencies and the spectral slope at $f > f_{peak}$ becomes flatter than in the source near a footpoint.

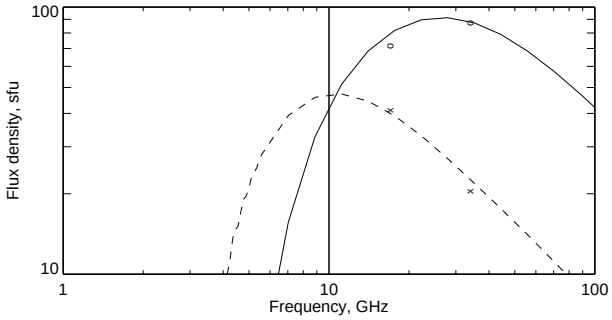

Fig. 13. Comparison of observed fluxes at 17 and 34 GHz from the loop top (circles) and footpoint (crosses) sources with 10" × 10" area and the corresponding microwave spectra calculated for these sources (Melnikov et al. 2005). The plasma density is assumed constant along the loop, $n_0 = 8 \times 10^{10}$ cm^{-3}, the magnetic field is 100 G and 200 G in the loop top and footpoint sources, respectively.

The fourth possible reason is a difference in energy spectrum slopes of electrons propagating in the looptop and footpoints regions. It is expected that the population of emitting electrons consists of two parts: trapped and directly precipitating into footpoints. The first part gives its contribution into microwave emission mainly in the looptop region while the second part in the footpoint regions. The energy spectrum of trapped electrons is supposed to be harder than of precipitating ones due to long lasting Coulomb interactions with the background plasma. Therefore, the frequency spectral slope of emission from the footpoints should be steeper. This idea may be exploited as an explanation of a better fit between electron spectra derived from microwaves and hard X-ray spectra coming from footpoints than from the looptop (see, for example, Kiyohara et al (2005)). However, it has to be checked by careful modeling with an use of the Fokker-Planck equation.

The observed temporal flattening of the microwave spectrum in its optically thin part is another interesting property. The flattening occurs throughout the loop-like source (from the loop top to the footpoints) in parallel with simultaneous softening of hard X-ray spectrum during the decay phase of bursts. Together with observed time delays at higher frequencies, these properties indicate on a different spectral behavior of low energy electrons generating hard X-ray emission and mildly relativistic electrons trapped in flaring loops and generating the microwave emission. The most probable explanation of this is that the hard X-ray emission is generated by directly precipitating electrons, and the microwaves mostly by trapped ones whose energy spectral evolution is defined by transport effects like Coulomb collisions (or wave-particle interactions) (Melnikov & Silva 2000). New properties of temporal behavior which may correct the explanation are the differences in the dynamics of flux and spectral slope of emissions coming from the top and footpoint parts of a flaring loop. They include: 1) slower intensity decay and time delays of microwave emission from the loop top part compared to the footpoint part; 2) faster

spectral flattening of emission from the footpoint part.

These spatial-temporal peculiarities, together with spatial dependence of the spectral slope, may be adjusted to each other if one takes into account the magnetic field inhomogeneity in a flaring loop. The physical reason for that is the following. The gyrosynchrotron emission at a given frequency from the loop top is generated at higher harmonics of gyrofrequency due to the lower magnetic field compared to the footpoint region. In its turn the emission at higher harmonics is generated by more energetic electrons that have a remarkably longer life time in the trap. The longer lifetime of these electrons explains naturally a) the slower intensity decay, b) the delays of emission and more gradual spectral flattening of emission from the loop top compared to the footpoints. Moreover, as it was mentioned earlier, the emission at higher harmonics also is expected to have flatter frequency spectrum that fits well with the observed flattening in the looptop.

Right now we can not exclude that some of the spatial-temporal properties of the frequency spectrum are caused by an acceleration mechanism itself. Before making firm conclusions all of them need to be carefully checked using self-consistent theoretical modeling and additional independent information on magnetic field strength, plasma density and electron energy spectrum in specific flaring loop.

4. Conclusion

Recent Nobeyama Radioheliograph observations reveal a set of new important spatial-spectral-temporal properties of microwave flaring loops. Among them are 1) the fact that the brightness distribution along flaring loops may have the maximum in the looptop even in the case of optically thin emission; 2) change of the initial distribution with brightness maxima near footpoints to the distribution with the looptop brightness maximum on the decay phase of a burst; 3) the existence of delays between the time profiles of emission from the loop top and footpoints; time delays at higher frequency; 4) the steepening of the microwave frequency spectrum along a loop from the top to its footpoints; 5) temporal flattening of the spectrum on the rise and decay phases of bursts; the faster flattening near footpoints than in the looptop on the decay phase.

Consideration of possible reasons explaining these properties reveal an importance of such effects as: 1) trapping and accumulation of accelerated electrons in the upper part of flaring loops, 2) transverse anisotropy of the electron pitch-angle distribution and its influence on the microwave intensity and spectral slope, 3) scattering of energetic electrons leading to a redistribution of electrons in a flaring loop and hardening of their energy spectrum, 4) Razin suppression and its influence on the microwave frequency spectrum, 5) dependence of the frequency spectrum slope on the magnetic field strength in a source. We should also emphasize an importance of the position of an acceleration/injection site inside a flaring loop. It greatly influences upon many observable spatial characteristics of microwave flaring loops.

So far we have not got sufficient information about the main effects which mostly responsible for the observed properties. We believe that relative significance of the listed effects may be determined only under complex, multi-wavelength and detailed case-studies of some specific flares.

All together the discussed findings put important new constraints on the particle acceleration/injection mechanisms and the kinetics of high energy electrons in flaring magnetic loops. We hope that future Nobeyama Radioheliograph observations will give us new excellent keys for solving problems of solar flare physics.

Acknowledgments

The work was partly supported by the RFBR grants No.04-02-39029, 04-02-16753. V.M. thanks the National Astronomical Observatory of Japan for the support of his visit to NRO. Author is also grateful to Drs. K.Shibasaki, V.Reznikova and S.Gorbikov for fruitful discussions, and to Drs. H.Nakajima and Y.Hanaoka for providing the corrected microwave data on the event of 2002, August 24 for use in this publication.

References

Alissandrakis, C.E., and Preka-Papadema, P. 1984, A&A, 139, 507
Aschwanden, M.J. 2002, Space Science Reviews, 101, 1
Bastian, T.S., Benz, A.O, & Gary, D.E. 1998, ARAA, 36, 131
Dulk, G. A. 1985, Ann. Rev. Astron. Astrophys., 23, 169
Fleishman, G. D., & Melnikov, V. F. 2003, ApJ, 587, 823
Fleishman, G. D., 2005 (this Proceedings)
Fletcher, L. 1999, ESA SP-448, 2, 693
Gorbikov G.D. & Melnikov V.F., 2005, *Mathematical Modeling* (in press)
Hamilton R.J., Lu E.T. & Petrosian V. 1990 ApJ, 354, 726
Hanaoka, Y. 1996, Sol. Phys., 165, 275
Hanaoka, Y. 1999, PASJ, 51, 483
Jakimiec, J. 2002, Proc. 10th European Solar Physics Meeting, Solar Variability: From Core to Outer Frontiers, Prague, Czech Republic, 645
Karlicky, M. & Kosugi, T. 2004, A&A, 419, 1159
Kawabata, K, et al. 1982, in "Proc. Hinotori Symp. on Solar Flares", eds. ... (Tokyo: ISAS), 168
Kiyohara, J., Takasaki, H., Narukage, N, Masuda, S., Nakajima, H., Yokoyama, T. 2005 (this Proceedings)
Klein, K.-L., and Trottet, G. 1984, A&A, 141, 67
Kundu, M., Schmall, E.J., & Velusamy, T. 1982, ApJ, 253, 963
Kundu, M.R., Nindos, A., White, S.M., and Grechnev, V.V. 2001, ApJ, 557, 880
Lee, J., and Gary, D.E. 2000, ApJ, 543, 457
Lee, J., Gary, D.E., Qiu, J., Gallacher, P.T. 2002, ApJ, 572, 609
Lee, J.W., Bong, S.C, & Yun, H.S. 2003, JKAS, 36, S63
Marsh, K.A., and Hurford, G.J. 1980, ApJ, 240, L111
Melnikov, V. F. 1994, Radiophys. & Quant.Electr., 37(7), 557
Melnikov, V.F., and Magun, A. 1998, Sol. Phys.., 178, 153
Melnikov, V.F., and Silva, A.V.R. 2000, ASP Conf. series, 206, 371, 475

Melnikov, V.F., Shibasaki, K., Yokoyama, T., Nakajima, H., and Reznikova, V.E. 2001, Abstracts of the CESRA workshop, July 2-6, 2001, Munich, Germany
Melnikov V.F., Shibasaki K. & Reznikova V.E. 2002a, ApJ, 580, L185
Melnikov, V.F., Yokoyama, T., Shibasaki, K., and Reznikova, V.E. 2002b, ESA SP-506, 339
Melnikov V.F., Reznikova V.E., Shibasaki K. & Nakariakov V.M., 2005, A&A, 439, 727
Miller, J.A., Cargill, P.J., Emsly, A.G. et al. 1997, GRL 102, No.A7, 14, 631
Nakajima, H. 1983, Sol. Phys., 86, 427
Nindos, A., Kundu, M. and White, S. 2001, Abstracts of the CESRA workshop, July 2-6, 2001, Munich, Germany
Nishio, M., Yaji, K., Kosugi, T., Nakajima, H., and Sakurai, T. 1997, ApJ, 489, 976
Nita, G. M., Gary, D. E., Lee, J. W. 2004, ApJ, 605, 528
Petrosian, V. 1982, ApJ, 255, L85
Petrosian, V., Donaghy, T. Q., & McTierman, J. M. 2002, ApJ, 569, 459
Preka-Papadema, P., and Alissandrakis, C.E. 1992, A&A, 257, 307
Ramaty, R. 1969, AJ, 158, 753
Razin, V.A. 1960, Izv. VUZov Radiofizika, 3, 921
Somov B.V.& Bogachev S.A. 2003, Astronomy Letters, 29, 621
Somov, B.V., and Kosugi, T. 1997, ApJ, 485, 859
Su, Y.N. & Huang, G.L., 2004, Sol. Phys., 219, 159
White, S., Kundu M., Garaimov V., Yokoyama, T., & Sato J. 2002, ApJ, 576, 505
Yokoyama, T. , Nakajima, H., Shibasaki, K., Melnikov, V.F., & Stepanov, A.V. 2002, ApJ, 576, L87
Zhou, A.H. Su, Y.N. & Huang, G.L. 2005, Sol. Phys., 226, 327